

## Supporting Information

### **One-for-All Intelligent Core-Shell Nanoparticles for Tumor-Specific Photothermal-Chemodynamic Synergistic Therapy**

Hongshuai Wu,<sup>‡a</sup> Dihai Gu,<sup>‡a</sup> Shengjin Xia,<sup>a</sup> Fanghui Chen,<sup>a</sup> Chaoqun You,<sup>\*,b</sup> Baiwang Sun<sup>\*,a</sup>

<sup>a</sup> *School of Chemistry and Chemical Engineering, Southeast University, Nanjing 211189, PR China. E-mail address: chmsunbw@seu.edu.cn*

<sup>b</sup> *Department of Forest Chemical Processing Engineering, Jiangsu Key Lab for the Chemistry and Utilization of Agro-Forest Biomass, College of Chemical Engineering, Nanjing Forestry University, Nanjing 210037, PR China. E-mail address: chemyoucq@njfu.edu.cn*

<sup>‡</sup> *These authors have contributed equally to the work.*

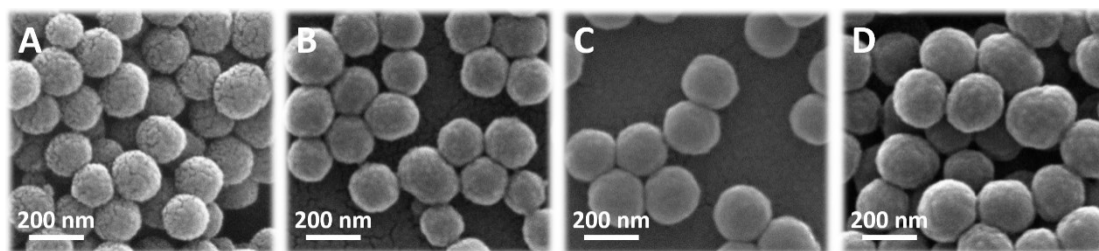


**Figure S1.** SEM images of (A) PDANPs, (B) PVP-PDANPs, (C) NH<sub>2</sub>-MIL@PDANPs and (D) HG-MIL@PDANPs.

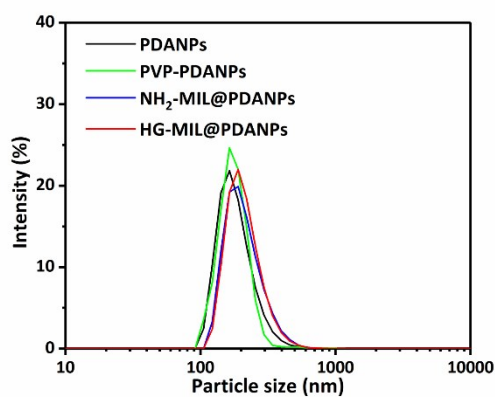


**Figure S2.** DLS size distribution of PDANPs, PVP-PDANPs, NH<sub>2</sub>-MIL@PDANPs and HG-MIL@PDANPs.

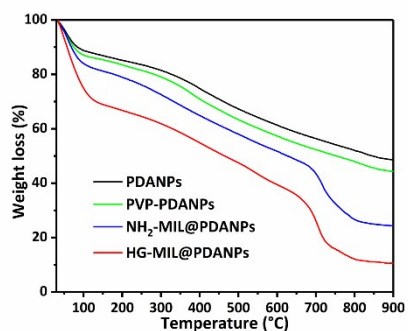


**Figure S3.** TGA curves of PDANPs, PVP-PDANPs, NH<sub>2</sub>-MIL@PDANPs and HG-MIL@PDANPs.

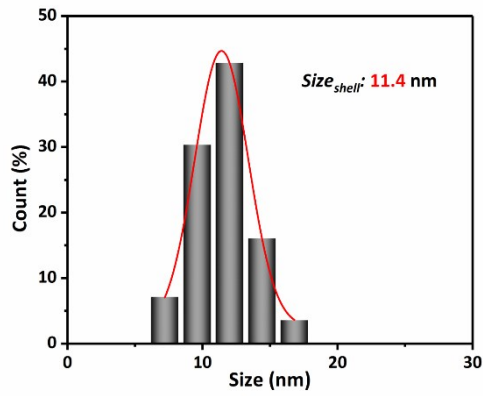


**Figure S4.** The size distribution of shell obtained from TEM image of NH<sub>2</sub>-MIL@PDANPs.

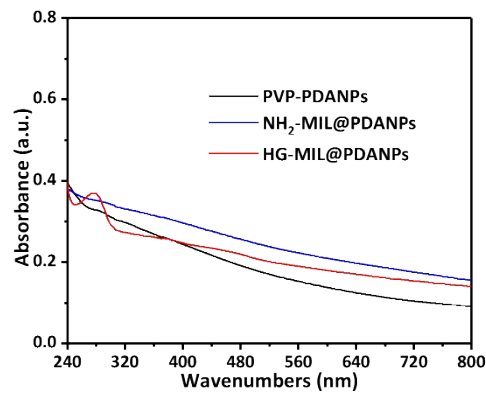


**Figure S5.** UV-vis spectra of PVP-PDANPs, NH<sub>2</sub>-MIL@PDANPs and HG-MIL@PDANPs.

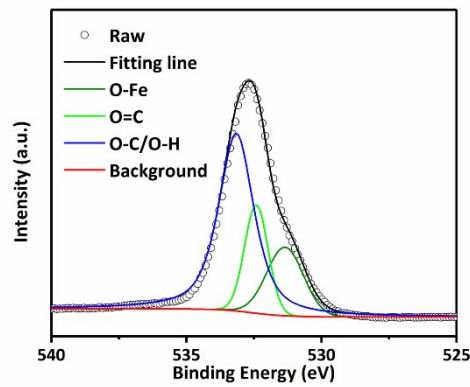


**Figure S6.** The high-resolution O XPS spectra of NH<sub>2</sub>-MIL@PDANPs.

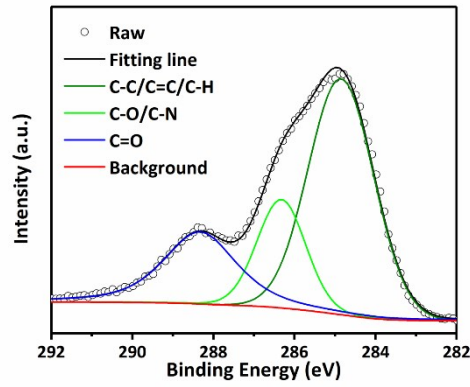


**Figure S7.** The high-resolution C XPS spectra of NH<sub>2</sub>-MIL@PDANPs.

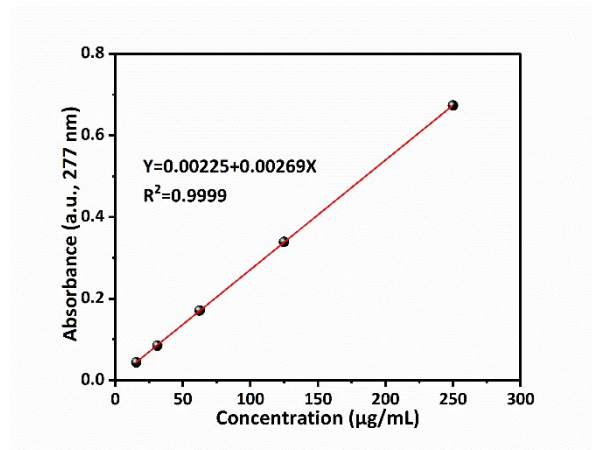


**Figure S8.** The standard curve of GOx.

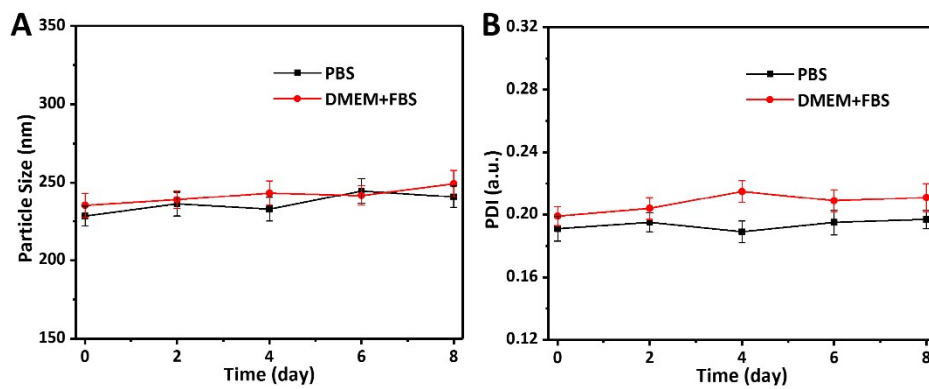


**Figure S9.** The (A) particle size and (B) PDI changes of HG-MIL@PDANPs in PBS and

10% FBS-supplemented RPMI with time.

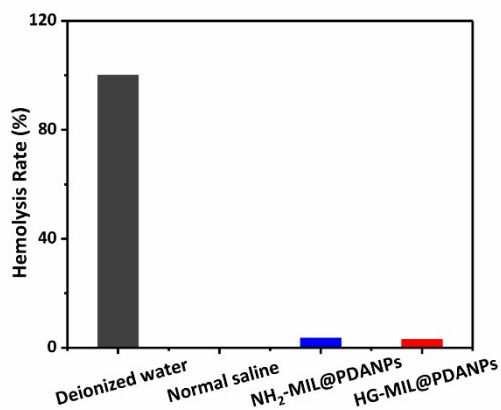


**Figure S10.** Hemolysis rate of deionized water, normal saline, NH<sub>2</sub>-MIL@PDANPs and HG-MIL@PDANPs.

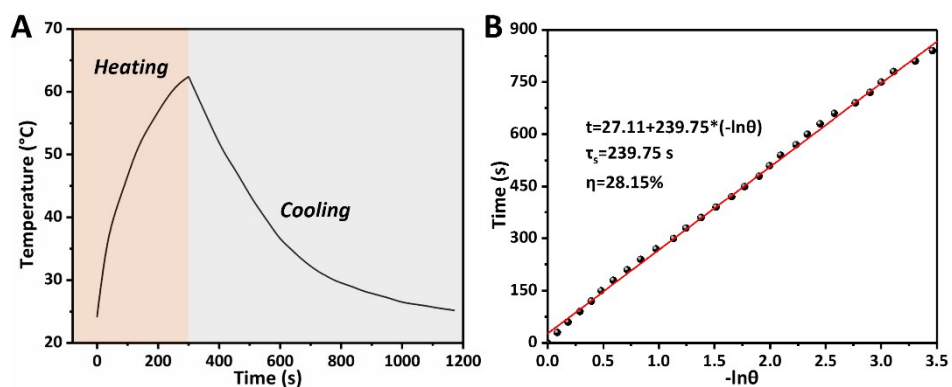


**Figure S11.** (A) Heating and cooling curve of PDANPs (50 μg mL<sup>-1</sup>) under 808 nm NIR irradiation. (B) Linear time data versus  $\ln\theta$  of PDANPs obtained from the cooling period.

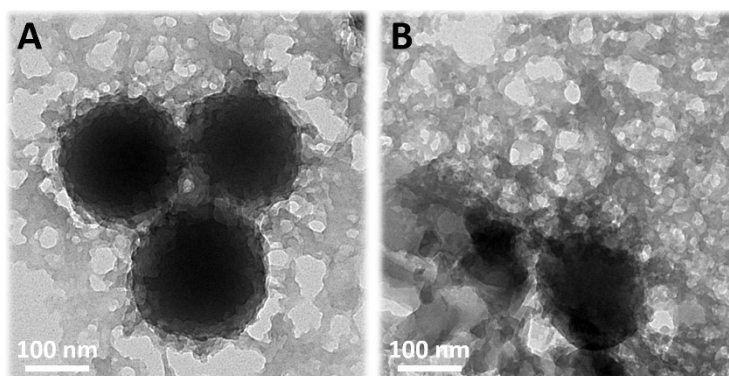


**Figure S12.** TEM images of HG-MIL@PDANPs after treatment of pH 5.0 (A) without

and (B) with 808 nm NIR irradiation for 5 min.

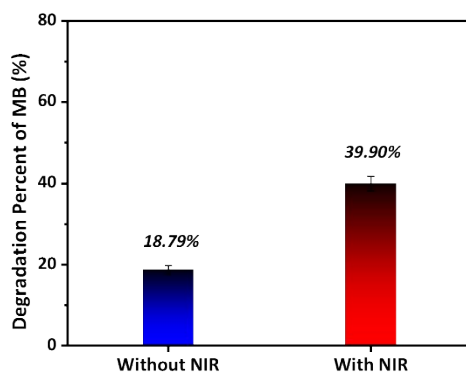


**Figure S13.** Degradation percent of MB incubated with  $\text{H}_2\text{O}_2$  plus acid-treated HG-MIL@PDANPs without and with 5 min of 808 nm NIR irradiation.

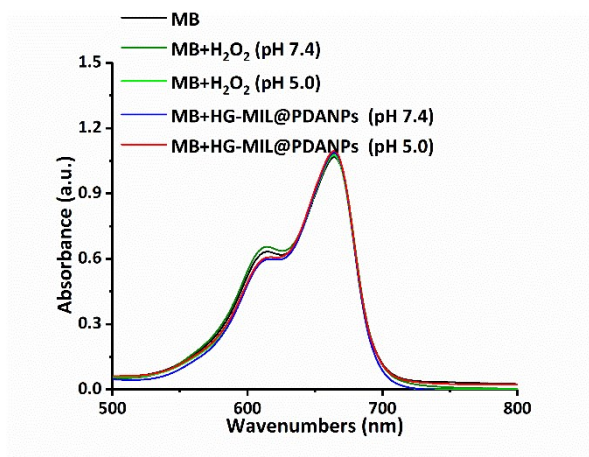


**Figure S14.** UV-vis spectra of MB incubated with single  $\text{H}_2\text{O}_2$  and  $\text{H}_2\text{O}_2$  plus HG-MIL@PDANPs after treatments with pH 7.4 and 5.0.

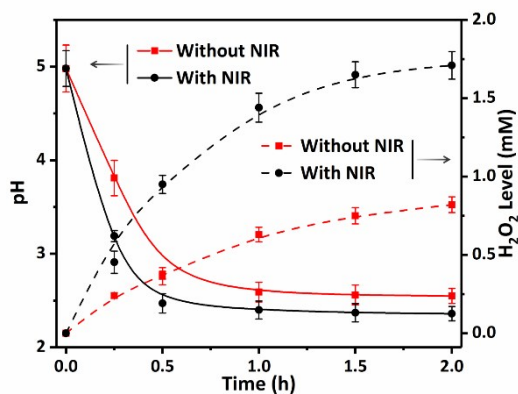


**Figure S15.** The pH values and generation of  $\text{H}_2\text{O}_2$  after incubation with glucose plus

acid-treated HG-MIL@PDANPs without and with 5 min of 808 nm NIR irradiation.

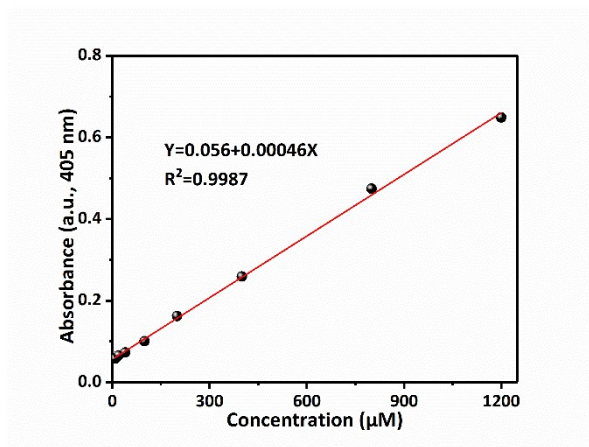


**Figure S16.** The standard curve of H<sub>2</sub>O<sub>2</sub>.

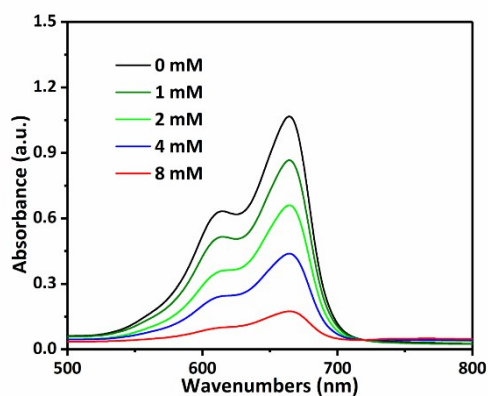


**Figure S17.** Degradation of MB by H<sub>2</sub>O<sub>2</sub> with different concentrations plus acid-treated HG-MIL@PDANPs.

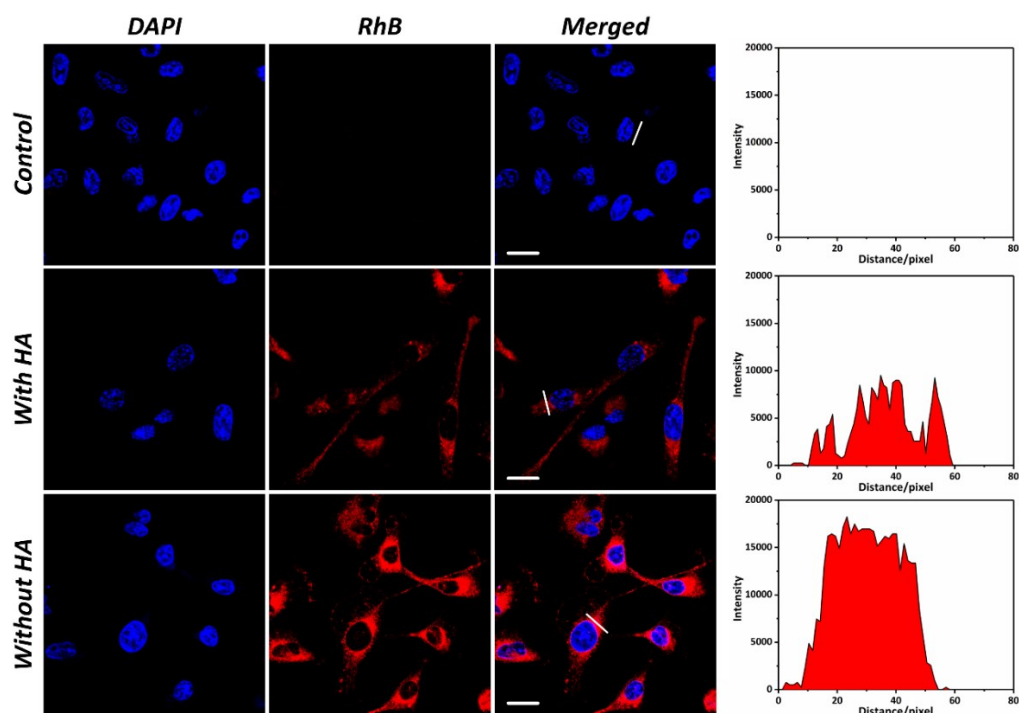


**Figure S18.** CLSM images and corresponding red fluorescence intensity profiles in MDA-MB-231 cells treated with RhB-doped HG-MIL@PDANPs for 4 h with and without HA pre-incubation. Scale bar: 20  $\mu\text{m}$ .

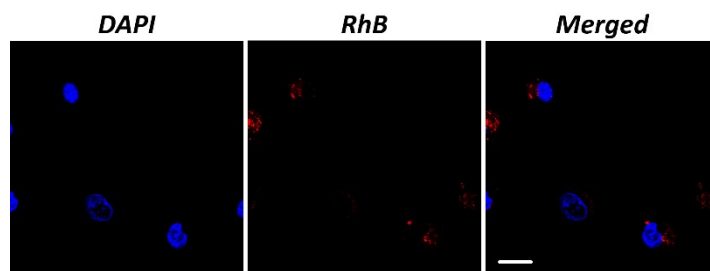


**Figure S19.** CLSM images of LO2 cells treated with RhB-doped HG-MIL@PDANPs for 4 h. Scale bar: 20  $\mu\text{m}$ .

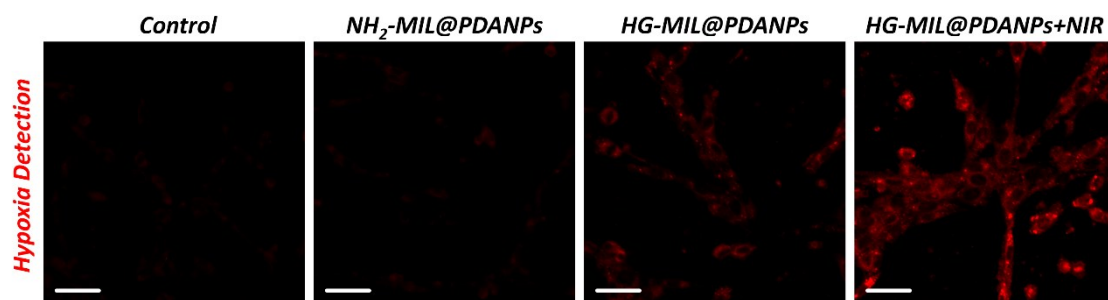


**Figure S20.** The CLSM images of hypoxia fluorescence in MDA-MB-231 cells after 12 h of incubation with  $\text{NH}_2\text{-MIL@PDANPs}$ ,  $\text{HG-MIL@PDANPs}$  and  $\text{HG-MIL@PDANPs}$  with 5 min of NIR irradiation. Scale bar: 40  $\mu\text{m}$ .

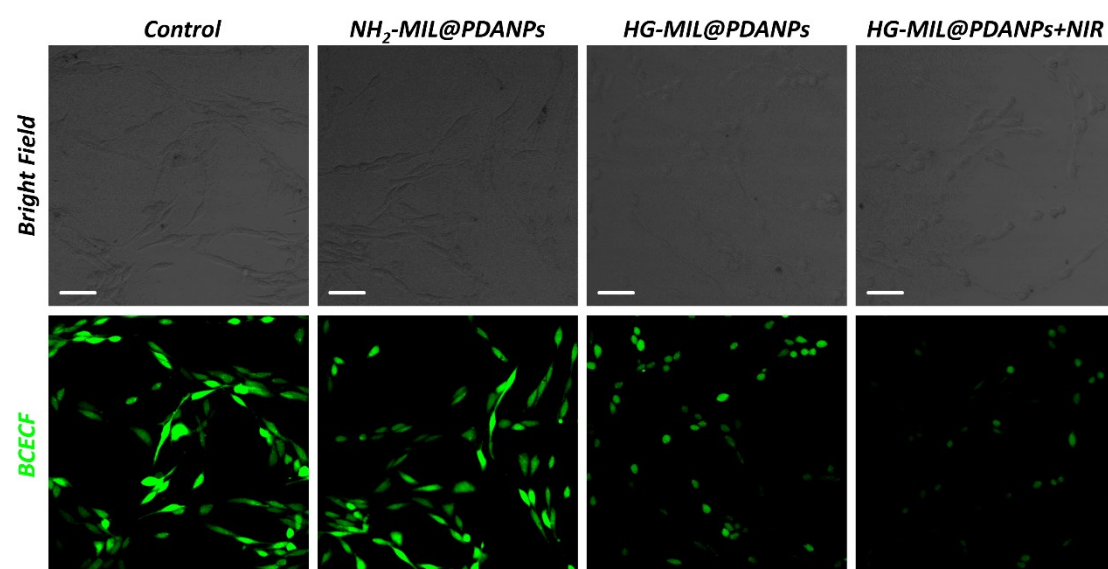


**Figure S21.** The CLSM images of BCECF fluorescence in MDA-MB-231 cells after 12 h of incubation with  $\text{NH}_2\text{-MIL@PDANPs}$ ,  $\text{HG-MIL@PDANPs}$  and  $\text{HG-MIL@PDANPs}$  with 5 min of NIR irradiation. Scale bar: 40  $\mu\text{m}$ .

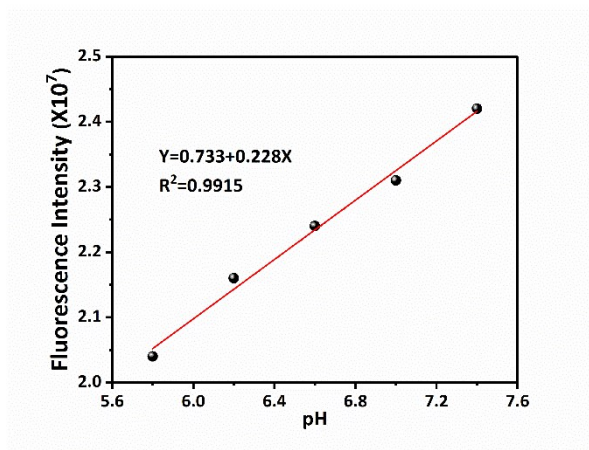


**Figure S22.** The standard curve of pH obtained by culturing cells at different acidic conditions.



**Figure S23.** Cell viability of MDA-MB-231 cells treated with NH<sub>2</sub>-MIL@PDANPs and HG-MIL@PDANPs for 24 h under the presence of glucose. n = 3, mean ± SD; \*\*, p < 0.01.

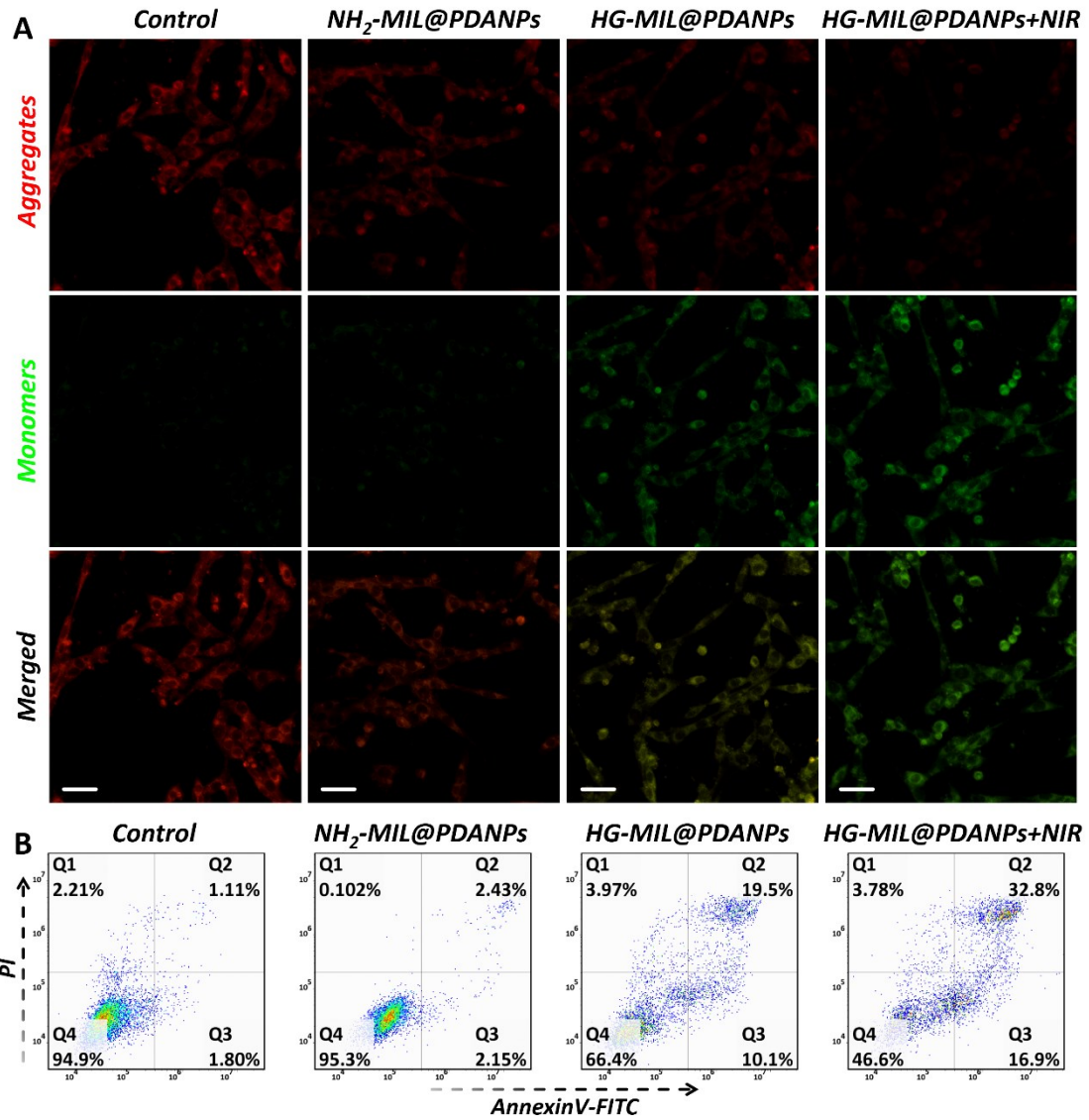


**Figure S24.** (A) Flow cytometry analysis of apoptosis and (B) CLSM images of JC-1 for MDA-MB-231 cells after the administrations of NH<sub>2</sub>-MIL@PDANPs, HG-MIL@PDANPs and HG-MIL@PDANPs with 5 min of 808 nm NIR irradiation. Scale bar: 40  $\mu$ m.

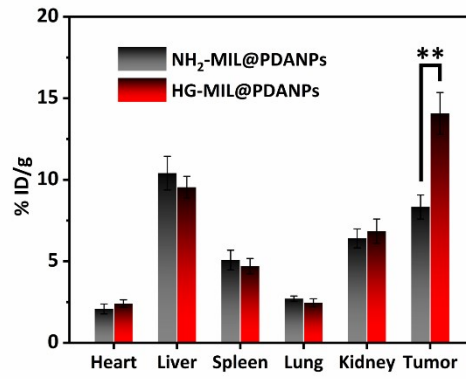


**Figure S25.** *In vivo* biodistribution of Fe in major organs and tumor after 24 h of post injection with NH<sub>2</sub>-MIL@PDANPs and HG-MIL@PDANPs. n = 3, mean ± SD; \*\*, p < 0.01.

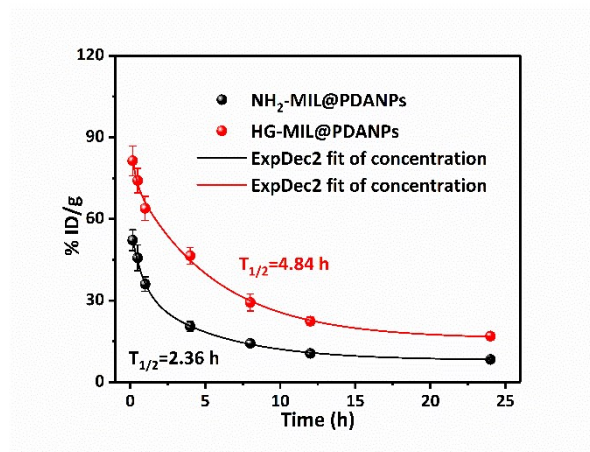


**Figure S26.** Blood-circulation lifetime of NH<sub>2</sub>-MIL@PDANPs and HG-MIL@PDANPs after intravenous injection.

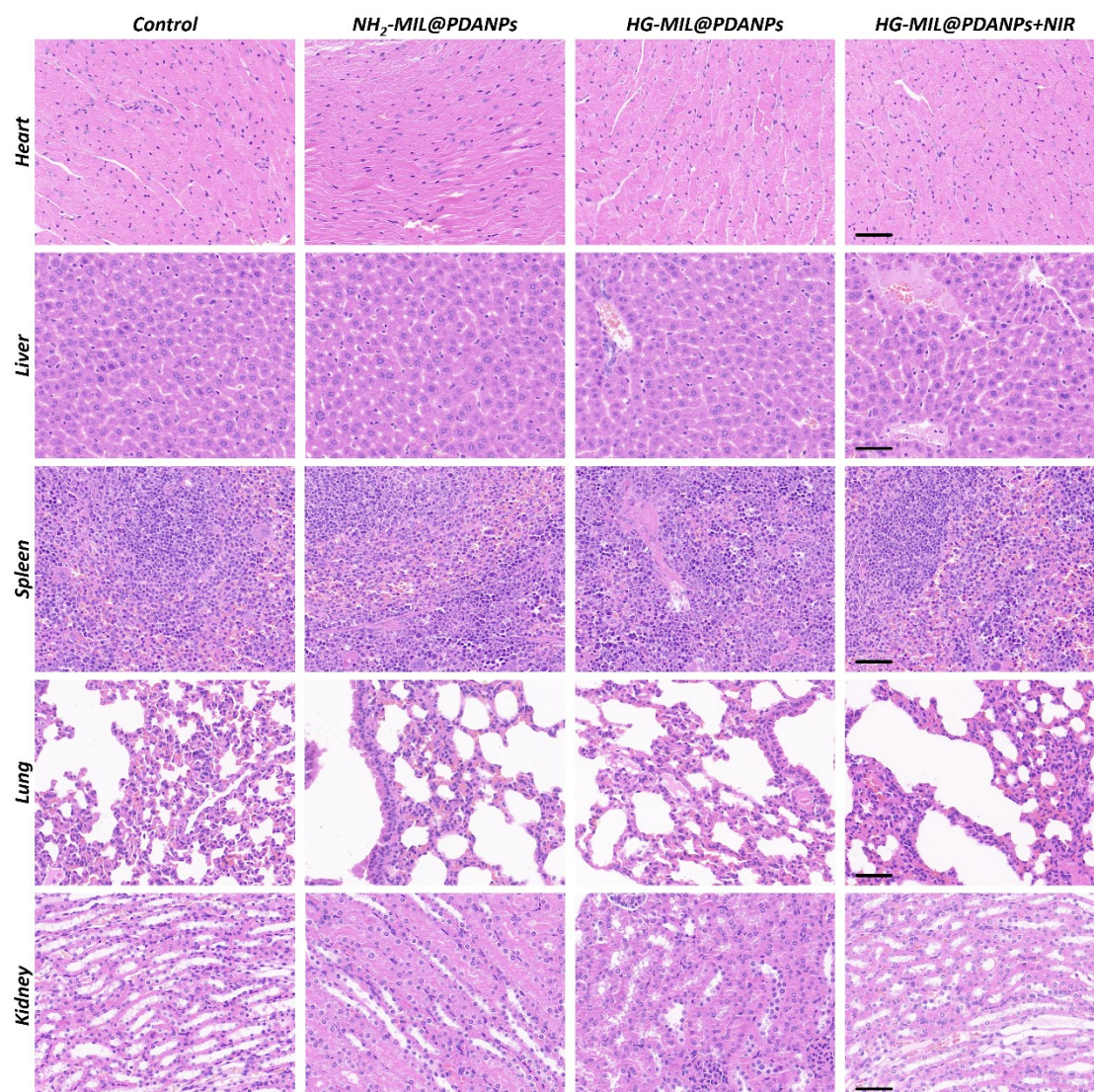


**Figure S27.** H&E staining of major organ slices after 15 days of different treatments. Scale bar: 50  $\mu$ m.